THE AMERICAN SOCIETY OF MECHANICAL ENGINEERS
Three Park Avenue, New York, N.Y. 10016-5990

99-GT-149

MODELLING OF A MICROSLIP FRICTION DAMPER SUBJECTED TO TRANSLATION AND ROTATION

GABOR CSABA
Volvo Aero Corporation
Military Engines
S-461 81 Trollhättan, Sweden

ABSTRACT

This paper presents a friction interface model where one of the mating surfaces is curved. The model is based on a discretization of the Winkler elastic foundation model and is general in the sense that it allows for relative motion in all six degrees of freedom. The variables for the contact model are based on damper geometry and material data, except coefficient of friction and tangential stiffness coefficient, which have to be measured. Simulated and experimental hysteresis curves are presented.

A model of a curved wedge damper has been developed using the contact model. An algorithm for solving forces and displacement when the damper is allowed to move in all six degrees of freedom has been presented. The governing algebraic equations are solved using a nonlinear least-square method routine in a commercial software package.

Forced response of a beam-damper-beam test set-up has been simulated and compared with experiments. The results highlighted some effects which have not been modelled e.g. the actual contact area between damper and blade is influenced by surface roughness for low normal loads. It is assumed that this effect resulted in problems in getting agreement between experiments and analysis. The influence of surface roughness is assumed to be negligible when vibrations of real turbomachinery are considered. This is due to the fact that both normal and excitation force on the damper are about ten times higher than what was used in the experiments and simulations in this paper.

Variation of contact radius of the damper shows that a larger radius e.g. a flatter contact gives better damping and increases the resonance frequency. The disadvantage is that the alignment of the damper becomes more unreliable.

INTRODUCTION

A common failure mode for turbomachinery is high-cycle fatigue of turbine blades, due to high dynamic stresses caused by blade vibration resonance within the operating range of the machinery. One method to reduce the dynamic stress is to increase the damping by use of dry friction in general, and specially a device called a platform friction damper. The damper is essentially a piece of metal which is fitted in a slot between the disk and platforms of two adjacent blades, as shown in Figure 1. The damper is pressed against the platforms by centrifugal

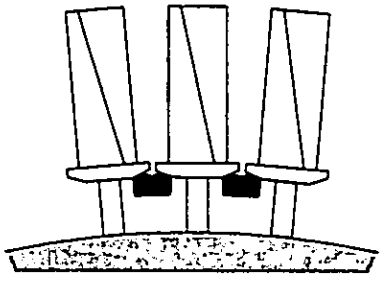

Figure 1 A part of a bladed disk with platform dampers.

force as the turbine rotates. Damping of blade vibrations and energy dissipation occur when there is slip in the contact between blade and damper. The most important factors that control the effectiveness of the friction damper are mass and coefficient of friction in the blade-damper contact, but stiffness and geometry are also important parameters. A good background and review of the subject of friction damping of turbine blade vibration is Griffin [1].

There are two theoretical approaches to modelling the friction interface between damper and blade platform, the macroslip and the microslip models. The entire friction interface is either stuck or is sliding in the macroslip approach. The onset of sliding is governed by Coulomb's law of friction. One of the first to study a dynamic system with Coulomb friction was den Hartog [2].

Presented at the International Gas Turbine & Aeroengine Congress & Exhibition
Indianapolis, Indiana — June 7–June 10, 1999

The most common macroslip model used to model friction dampers, proposed by Griffin [3], is shown in Figure 2.

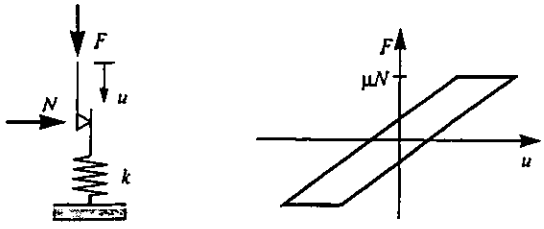

Figure 2 Macroslip friction interface model and corresponding hysteresis curve.

The model consists of a simple Coulomb point contact in series with a spring with stiffness k. This model is also named a bi-linear element after the shape of the hysteresis curve. The greatest advantage of the macroslip approach is that it is quite straightforward compared with the microslip theory. This is probably the reason why this method is the most frequently used in analysis of blade vibration. There are several disadvantages of the macroslip model. The approximation that all bodies in contact are rigid is in many cases not valid, especially if the contact pressure is high and displacements are small.

In the microslip approach the elasticity of members in contact is included, which leads to a slip zone that will gradually extend inwards through the damper before the interface reaches macroslip. This is a more physically motivated method to use since normal forces are high and displacements are small in blade vibration. Friction models that include microslip have been derived since the 1950's, Mindlin *et al.* [4] and Metherell and Diller [5]. The model in [5], here named the Bar model, has later been used as a friction damper model by Menq *et al.* [6] and Csaba [7]. The Bar model, shown in Figure 3 is a simple microslip model, yet complete enough to show the most important properties of microslip.

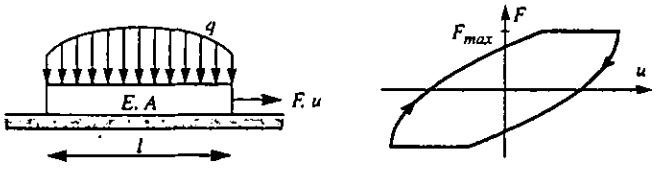

Figure 3 Microslip friction interface model and corresponding hysteresis curve.

The Bar model has been used successfully to model a commercially used damper, Csaba [8], and then optimized with respect to mass using simulations and spin-pit experiments by Csaba and Andersson [9].

There is one important disadvantage with the Bar model. There is no direct coupling between the geometry of most actual dampers and the variables of the Bar model, which are: cross-section area A and damper length l. These parameters have to be defined *ad hoc* or by some sort of curve fitting. Another limitation is that slip motion of the Bar model is one-dimensional. The relative motion between blade and damper runs forward and back along a straight line. There are many applications were the relative motion is two-dimensional, if for instance the blade is vibrating in a combination of bending and torsional modes, Srinivasan and Cutts [10]. Interface models for two-dimensional slip have been developed by Menq *et al.* [11] for macroslip and by Sanliturk and Ewins [12] and Sextro *et al.* [13] for microslip.

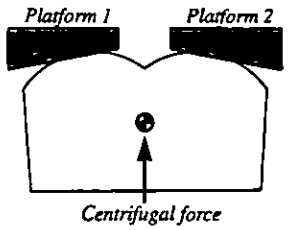

Figure 4 Damper configuration.

A closer view of the configuration for a curved wedge damper is shown in Figure 4. One characteristic of this configuration is that the platforms are inclined. This makes the damper self-centring when centrifugal load is applied. Another characteristic is that the contact surface of the damper is curved, which allows rolling motion of the damper. Pfeiffer and Hajek [14] have used a macroslip contact model to analyse and optimize a damper with parabolic configuration and rolling motion. A wedge damper with flat contact surface, also called cottage roof damper, has been modelled by Yang and Menq [15], [16]. They used the bi-linear macroslip element for the contact between damper and blade platform. Sanliturk *et al.* [17] have also developed a cottage roof damper model using the microslip friction interface in [12].

The first objective of this paper is to develop a microslip interface model for the contact between the platform and a curved damper, which is general in the sense that it allows for relative motion in all six degrees of freedom, DOF. The second objective is to use the interface model to make a model of a commercially used damper and to compare simulations with experiments

FRICTION INTERFACE MODEL

Consider two elastic bodies in contact subjected to normal and tangential force. The friction force and displacement at a certain point is influenced by the normal stress on the whole contact interface. An elastic problem such as this has to be solved using the finite element method, FEM. One may simplify the contact problem by assuming a nonlocal friction law, where the friction force at a point is influenced by the normal stress over a neighbourhood, Srinivasan and Cassenti have defined such a law in [18]. This type of friction law is faster in computation time compared with FEM, but with the speed of computers available today, still not feasible if dynamic analysis of complex structures are considered.

A contact model which is a discretized version of the Winkler elastic foundation model is presented in this section. The simplified model is governed by a local friction law i.e. the friction force on a point in contact is only influenced by the normal load on that point. The adoption of a local friction law saves computation time compared with a nonlocal law. The Winkler elastic foundation model has also recently been used by Põdra and Andersson [19] for wear simulations and showed good agreement compared with finite element analysis.

The Brush Model

The Winkler elastic foundation model, Johnson [20], consists of two rigid bodies, a plane and an indenter, with an elastic foundation in between them. The model proposed here, shown in Figure 5, is a discretized version of the Winkler model and named the Brush model. The elastic foundation is discretized into an array of $n_x \times n_y$ bristles

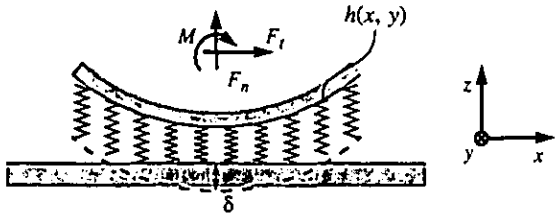

Figure 5 The Brush model, schematic view in two dimensions.

which are modelled as linear springs with equal unloaded length. The plane simulates a part of the blade platform and the indenter simulates a part of the damper. Bristles are fixed to the indenter and, if in contact with the plane, governed by Coulomb's law of friction for a point contact. Assuming that contact area is small compared with the bodies in contact, the indenter curvature is defined as

$$h(x, y) = x^2/(2r_x) + y^2/(2r_y) \tag{1}$$

where r_x and r_y are radii of curvature. The indenter may be moved in all six DOF (three translations and three rotations). A normal displacement of the indenter δ associated with a normal force F_n will make the bristles come into contact, shown as filled circles in Figure 6. One should note that the normal force in Figure 5 is negative due to definition of coordinate system. The grey area shows where the indenter has entered the elastic foundation.

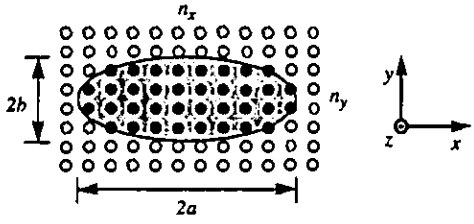

Figure 6 A mesh of n_x by n_y bristles, where loaded bristles are shown as filled circles. The area where the indenter is in contact with the foundation is shown in grey.

The Brush model is similar to those presented by Sanliturk and Ewins [12] and Sextro *et al.* [13] in the sense that they all use an array of macroslip elements to describe a microslip contact model. The Brush model is, however, more general as it allows for relative motion in all six degrees of freedom, while the other two do not model rotation and displacement normal to the contact, although these effects are incorporated empirically in Sanliturk *et al.* [17]. Another important difference is that the Sanliturk model is based on experimentally-measured one-dimensional hysteresis curves.

Properties of a bristle

A schematic view of a bristle is shown in Figure 7. It has a normal stiffness k_n and a lateral stiffness k_t. The values of k_n and k_t are found by comparing pressure and contact area for the Hertzian solution to the contact problem with the Brush model solution. The bristle stiffness may according to [20] be defined as

$$k_n = \gamma_n E^* A/b \tag{2}$$

$$k_t = \gamma_t E^* A/b \tag{3}$$

Figure 7 Definition of bristle normal and tangential stiffness.

where b is the shorter semi-axis from the Hertzian solution, A is the contact area associated with a bristle, γ_n and γ_t are nondimensional stiffness coefficients. With E and ν being material modulus of elasticity and Poisson's ration respectively, the combined modulus E^* is defined as

$$\frac{1}{E^*} = \frac{1-\nu_1^2}{E_1} + \frac{1-\nu_2^2}{E_2} \tag{4}$$

Using Eq. (1) to define the curvature of the indenter gives a shape of the pressure curve that is quadratic while the a Hertzian contact without friction gives a pressure curve with an elliptic shape. This leads to the fact that it is not possible to get the same maximum pressure and contact area for the two contact models. It is assumed here that it is more important to have the same contact area. Depending on the shape of the indenter i.e., r_x/r_y, γ_n is computed to give equal contact area. The two extreme cases are the axi-symmetric point contact and the two-dimensional line contact, which give $\gamma_n = 1.70$ and $\gamma_n = 1.18$ respectively. One may for the general case use $\gamma_n = 1.35$, which leads to an error in length of the shorter semi-axis not exceeding 7% for either line or point contact [20]. A thorough discussion about this parameter may be found in [19]. It is more difficult to find an appropriate value for the tangential stiffness coefficient γ_t. This parameter is largely influenced by how we define the contact bodies and how far away from the contact we measure/compute the relative displacement. Johnson [20] suggests that setting $\gamma_t = 2/3\gamma_n$ is an appropriate values for a general case. This will be compared with experiment in a later section.

Forces and displacements for the Brush model

We define a mesh with $n_x + 1$ by $n_y + 1$ bristles as shown in Figure 8. The two variables defining the mesh size l_x and l_y should be large enough to cover the potential contact area, see Figure 6 and also allow for the contact area to move if the damper is rolling.

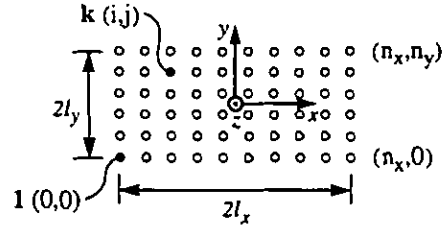

Figure 8 Definition of bristle co-ordinate system.

A discretized coordinate frame is defined as

$$x(i) = l_x(2i/n_x - 1), \quad i = 0, 1, \ldots n_x \tag{5}$$

$$y(j) = l_y(2j/n_y - 1), \quad j = 0, 1, \ldots n_y \tag{6}$$

There are two variables defining bristle displacements, v and w as shown in Figure 9. The variable v defines the points where bristles are attached and fixed to the indenter. The variable w defines coordinates and displacements of contact points between bristles and the plane.

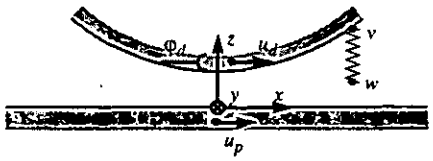

Figure 9 Displacement and rotation coordinates for Brush interface model.

The contact point displacement is set to be equal to attachment displacement for unloaded bristles. This implies that the friction force will be zero when a bristle comes into contact

A matrix $[v_0]$ containing the coordinates for bristle attachment is defined using homogenous coordinates. Index 0 indicates that the indenter displacement is zero. The position of a bristle is stored in a row with index $k = 1 + jn_x + i$. The elements of a row k are

$$v_0(k, 1) = x(i)$$

$$v_0(k, 2) = y(j)$$

$$v_0(k, 3) = h(x(i), y(j))$$

$$v_0(k, 4) = 1$$

The element of column 4 is a scale factor and is normally set to unity. If we consider rotation and translation of bristles then the former is a matrix multiplication and the latter is an addition. The benefit of using homogenous coordinates is that all matrix operations may be treated as a series of multiplications. One may also premultiply all operation matrices together before applying them to the bristle matrix. This is advantageous when computation time is concemed, Pärletun *et al.* [21]. The translation matrix is defined as

$$[T] = \begin{bmatrix} 1 & 0 & 0 & 0 \\ 0 & 1 & 0 & 0 \\ 0 & 0 & 1 & 0 \\ T_x & T_y & T_z & 1 \end{bmatrix} \tag{7}$$

Standard rotational matrices are used, but with an extra element as shown below for R_x

$$[R_x(\varphi_x)] = \begin{bmatrix} 1 & 0 & 0 & 0 \\ 0 & \cos\varphi_x & \sin\varphi_x & 0 \\ 0 & -\sin\varphi_x & \cos\varphi_x & 0 \\ 0 & 0 & 0 & 1 \end{bmatrix} \tag{8}$$

The total rotation matrix $[R(\varphi)]$ is defined as

$$[R(\varphi)] = [R_x(\varphi_x)][R_y(\varphi_y)][R_z(\varphi_z)] \tag{9}$$

Rotation matrices $[R_x]$, $[R_y]$ and $[R_z]$ may be applied in any order, as long as one is consistent. If we apply a rotation and a translation to the indenter, then new positions for attachment points are defined as

$$[v] = [v_0][R(\varphi)][T] \tag{10}$$

A matrix $[w]$ is also defined for bristle contact points. This matrix contains two rows since the z-coordinate is equal to zero and the contact points have only tangential displacement.

Definition of platform and damper displacement u_p, u_d and damper rotation φ_d at the interface is shown in Figure 9. The figure shows only x- and z-displacement and y-rotation, but motions in all six degrees of freedom are allowed. The plane is fixed for rotational motion. Rotation of blade platforms in positive direction is instead treated as indenter rotation in the negative direction. To make computation of bristle forces simpler, we define a gap vector

$$g(k) = u_{pz} - v(k, 3) \tag{11}$$

This implies that $g(k) < 0$ for loaded bristles and hence forces and displacement are only computed for these elements. The normal force on one bristle is found as

$$f_n(k) = \begin{cases} k_n g(k) & \text{if } g(k) < 0 \\ 0 & \text{otherwise} \end{cases} \tag{12}$$

It is found, using Eqs (2), (11) and (12), that the bristle stiffness k_n is a nonlinear function of the normal load on the interface, which in a dynamic analysis may be varying. It is not feasible to have a variable bristle stiffness and the dynamic part of the normal load is normally small compared with the static part, which is caused by the centrifugal force on the damper. Bristle stiffnesses are therefore linearized around the static normal load on the interface.

The friction interface is in the general case subjected to a platform displacement u_p, the damper is displaced u_d and rotated φ_d. Bristle displacements and forces are then found using the algorithm in Figure 10. Note that the rotation and translation of bristle attachment matrix $[v]$ is rather complex, due to the definition of coordinate systems. We see in Figure 10 that damper displacement u_d and rotation φ_d are input variables. These are, however, in the general case unknowns and the contact problem has to be solved by iteration for a known quantity, say for instance the normal force F_n. It may be noted here that forces on contact points do not effect each other due to the fact that bristle deformation is uncoupled.

The applied normal load is found as the sum of bristle forces

$$F_n = \sum_k f_n(k) \tag{13}$$

It may be noted that the normal force on the interface is always negative according to definition of coordinates.The traction force is the sum of bristle friction forces

$$F_{t,x} = \sum_k f_t(k, 1) \tag{14}$$

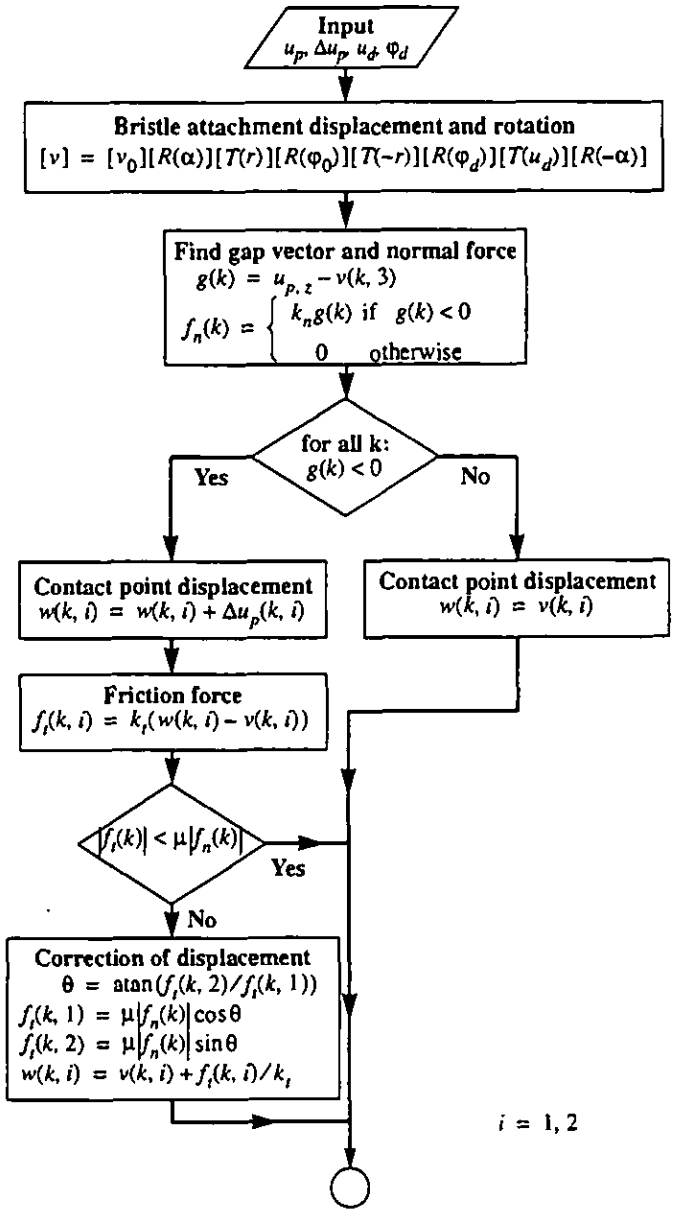

Figure 10 Algorithm for solving bristle force and displacement.

$$F_{t,y} = \sum_k f_t(k, 2) \tag{15}$$

The applied moment is found as

$$M_x = \sum_k f_n(k) w(k, 2) \tag{16}$$

$$M_y = \sum_k -f_n(k) w(k, 1) \tag{17}$$

$$M_z = \sum_k f_t(k, 2) w(k, 1) - \sum_k f_t(k, 1) w(k, 2) \tag{18}$$

SIMULATIONS AND VERIFICATION OF CONTACT MODEL

In this section we will do simulations with the Brush model to show the properties and also present experimental verification of the model.

One-dimensional hysteresis

An important characteristic of a friction interface model, the associated hysteresis curve, is found by applying a periodic displacement, which is monotonic between its peak values, to the interface and plotting the friction force against the displacement as shown in Figure 11.

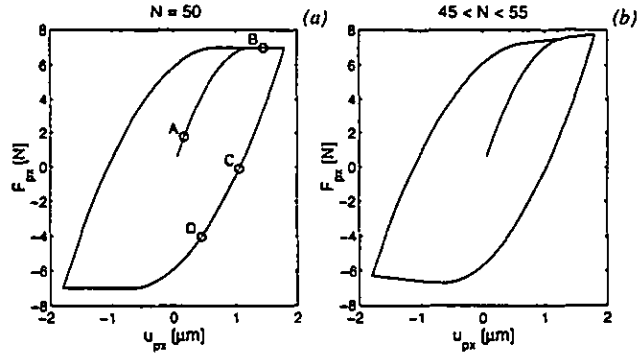

Figure 11 Hysteresis of one friction contact for constant and variable normal load.

Simulation data used in this section are:

$n_x = n_y = 21$, $r_x = 25$ mm, $r_y = 2.5$ mm, $l_x = 0.3$ mm, $l_y = 0.1$ mm, $N = 50$N, $\mu = 0.14$, $u_{px} = 1.8\sin(\theta)$ mm

The friction joint is in this simulation subjected to one-dimensional (1D) slip motion e.g. the relative displacement between indenter and plane follows a line. We see in Figure 11a that the hysteresis is symmetric for this type of motion. The unloading curve (u decreases from 1.8 to -1.8 μm) is a mirror image of the loading curve (u increases from -1.8 to 1.8 μm). This is the kind of hysteresis curve we see in most textbooks on friction or material damping and it may be derived from the initial loading curve using Massing rules, see Menq *et al.* [6] or Iwan [22].

Four points of the hysteresis loop are marked in Figure 11a. The friction force acting on the bristles corresponding to these points is displayed in Figure 12, plots *A* - *D*. Each arrow shows the magnitude and direction of the friction force acting on a bristle. Plot *A* shows friction forces at the beginning of initial loading. Almost all bristles have equal force except a few at the periphery which have already reached maximum friction force and are slipping. The state where we have gross slip is shown in plot *B*. The curvature of the indenter and the level of penetration give the normal force distribution and this is reflected in the limiting friction force shown in this plot. How bristle forces changes when we unload the interface is shown in plots *C* and *D*. We see in plot *C* that some bristles around the periphery have reached macroslip in the opposite direction to previously. Friction forces on bristles with high normal load (in the centre of the interface) have only increased, but do not change sign until the state shown in plot *D*.

The hysteresis curve is no longer symmetric and Massing rules do not apply if the normal load on the interface is varying with the displacement as shown in the right curve of Figure 11b. The normal load is in this simulation a function of displacement u_{px}, where maximum displacement gives maximum normal force. This was accomplished by

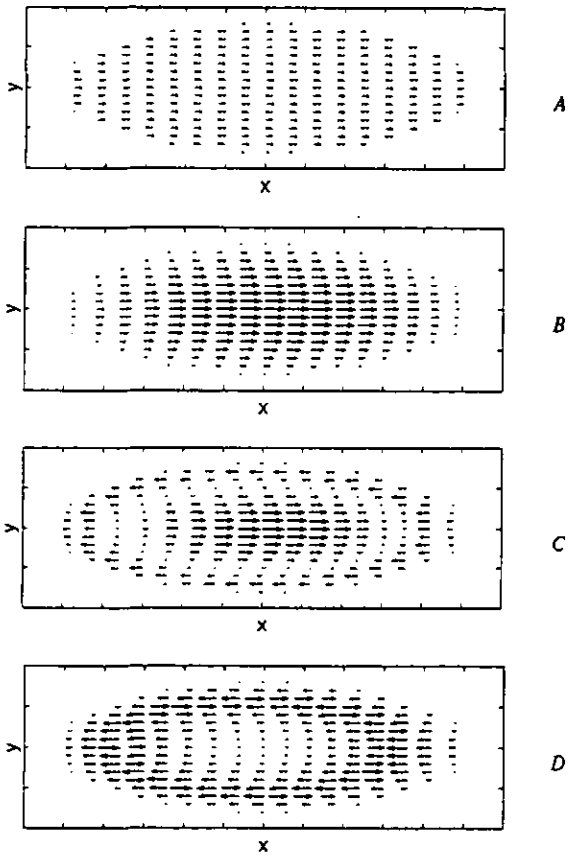

Figure 12 Mesh of bristle friction force for constant normal load simulation.

using the same simulation data as before but adding a normal displacement $u_{pz} = 0.07\sin(\theta)$ mm to the plane. A variable normal force results in the friction force no longer being constant when there is macroslip. An application where the normal load is varying is shrouded fan and turbine blades. This has been considered by Menq *et al.* [23] for microslip and Yang and Menq [24] for macroslip. Variable normal load in the case of a wedge [15] or a curved wedge damper is induced by the contact angle between damper and blade platform, resulting in the friction force affecting the normal force.

Another capability of the Brush model, besides variable normal load, is that there may be rolling motion in the contact. The friction interface was in this simulation subjected to a platform displacement $u_{px} = 1.8\sin(\theta)$, and a rotation $\varphi_{py} = 0.4°\sin(\theta)$. This type of motion is found for bending mode vibrations of turbine blades. The blade platform will perform a tangential displacement and a rotation at the same time. There will also be a radial displacement at the damper-blade contact, but this is not included in this simulation. The resulting hysteresis loop is shown in Figure 13 and associated bristle forces are shown in Figure 14.

The rolling motion will for this simulation case add an extra relative displacement between the indenter and the plane. The result is that the case with rolling in the contact will reach macroslip at an earlier state than the case without rolling. The associated hysteresis curves are shown as solid and broken lines in Figure 13. If we compare the mesh of bristle friction forces in Figure 14 with the ones in Figure 12, we see of

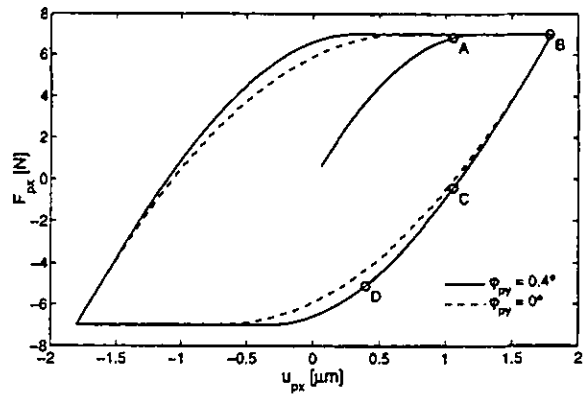

Figure 13 Hysteresis for the Brush model with and without rotation φ_y being present.

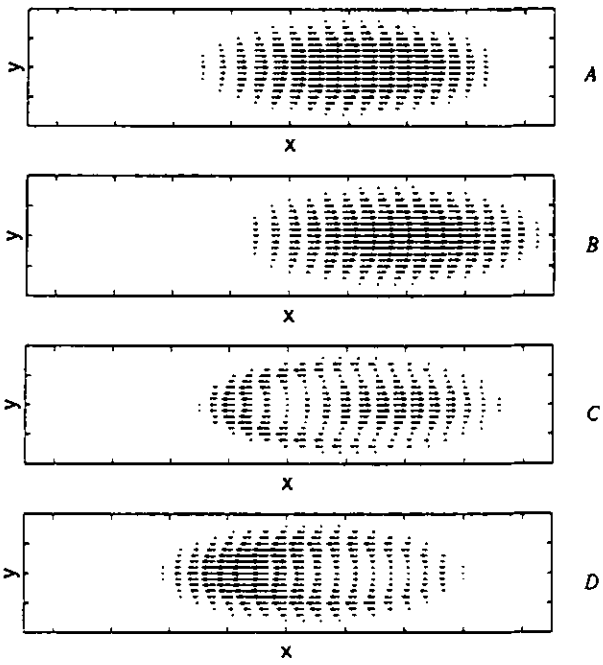

Figure 14 Mesh of bristles friction force for simulation with rolling.

course that the area of contact is translating due to the rolling. We see in Figure 12 that the bristle force magnitude is symmetric with respect to the centre of the contact area, but that is not the case in Figure 14. This is due to the fact that a bristle is unloaded when it comes into contact as defined in Eq. (11) and Eq. (12).

Two-dimensional hysteresis

The Brush model can also simulate two-dimensional (2D) slip motion. The relative motion between indenter and plane will now be an ellipse. Trajectories for individual bristles may or may not be elliptic, depending on normal load. The resulting hysteresis is shown in Figure 15. Data are the same as the first simulation, except that we have added a displacement $u_{py} = 0.3\sin(\theta + \beta)$, where β is the phase angle between x and y displacements. We see in Figure 15 that a phase angle of zero does not give 2D-slip, but 1D-slip along a line in the x-y-plane.

The shape of the hysteresis curves depends on the phase angle, as we see in the figure, and also on the relationship between $\hat{u}_{px}/\hat{u}_{py}$, which is equal to 3 for this case.

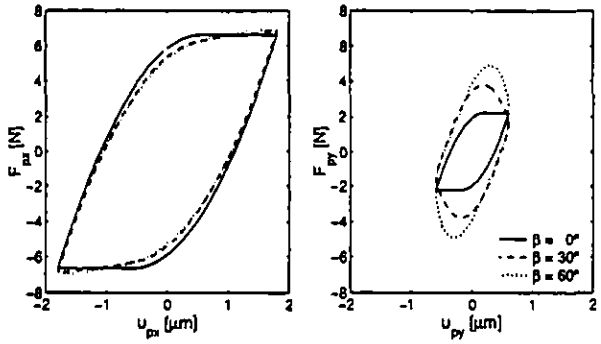

Figure 15 Hysteresis associated with 2D slip motion.

Measurement and verification of hysteresis curve

A technique for measuring hysteresis curves is developed at *Centre of Vibration Engineering* at *Imperial College, London U.K.* Some of the measured hysteresis curves are presented in this section in order to verify the contact model.

The basic method of how hysteresis loops are measured at IC has been presented by Sanliturk *et al.* [25]. The most important difference with this rig is that measurement of relative motion in the contact has been improved by using a laser-doppler vibrometer. It should be noted that the results are only preliminary and the measuring technique is still being refined. The rig has been presented in an internal report by Stanbridge.

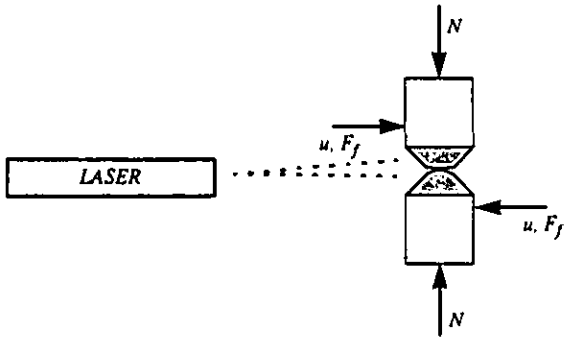

Figure 16 Measurement of hysteresis curves.

A schematic figure of the experimental set-up is shown in Figure 16. The two test specimens, one with flat contact surface and the other with curved surface, were pressed against each other and then subjected to one-dimensional relative displacement which was measured via a laser-doppler vibrometer. The friction force was measured with force transducers. Resulting hysteresis plots are shown in Figure 17. The two test specimens are made of a nickel alloy and experiments were conducted at room temperature so that results could be used in the blade-damper-blade case study described later on in this paper.

The objectives of the experiments were to verify the tangential stiffness coefficient γ_t and to measure the coefficient of friction μ. These two variables were varied so that the simulated and the measured curves in Figure 17a agree as well as possible. The variables were found to be $\gamma_t = 0.15$ and $\mu = 0.18$ when the normal force is $N = 5$N. Variable γ_t was then kept at the assigned value when curves in Figure 17b were fitted. The coefficient of friction was here found to be $\mu = 0.14$ when $N = 49$N.

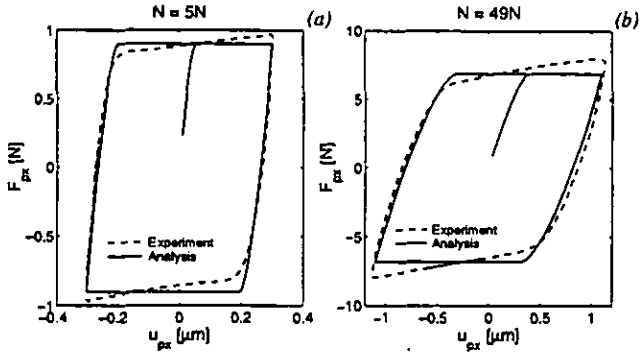

Figure 17 Comparison of measured and simulated hysteresis curves.

Results show that simulated hysteresis curves agree well with the measured ones in the microslip region. The tangential stiffness coefficient was found to be considerably less than suggested by Johnson [20]. This stiffness is, however, very difficult to determine. The result is largely influenced by how far apart the points are where relative displacement is measured.

It is seen in Figure 17 that the friction force F_{px} is constant during macroslip in the simulated hysteresis curves, while the measured curves shows that the friction force is not constant. The simulated hysteresis has one-dimensional slip and the measured hysteresis is assumed to have the same. It is observed, by comparing measured curves in Figure 17 with simulated ones in Figure 15, that they show resemblance. This implies that there is possibly two-dimensional slip between the test specimens in the experiment. The hypothesis of 2D-slip is currently under investigation at Imperial College.

A SIX-DEGREES-OF-FREEDOM DAMPER MODEL

We will in this section derive governing equations for a curved wedge damper. There are two damper-platform contact areas named C_1 and C_2. Each of them is modelled using a Brush interface model. The "body" of the damper is also considered as elastic and modelled with spring elements. A schematic view of the damper model is shown in Figure 18. The figure also shows how coordinate systems are defined.

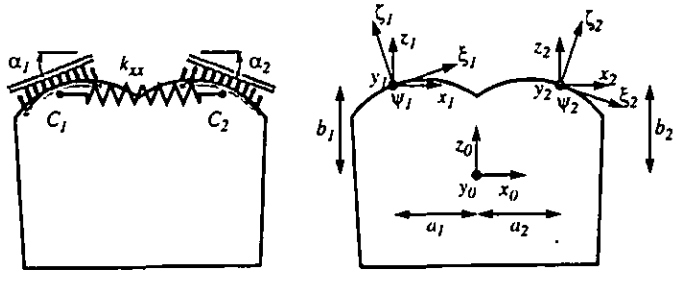

Figure 18 Coordinate systems for an elastic curved wedge damper.

The global x,y,z-systems, indexed 0, has its origin in the damper centre of gravity (C.G.). Two local co-ordinate systems, indexed 1 and 2, have origin at blade-damper contact. Each contact also has a local system where coordinate ζ is normal to the contact surface. The blade platform inclination angle is denoted α.

Forces and Displacements

Forces and moments on the damper are defined as:

$$\{F_l\} = \{F_{lx}\ F_{ly}\ F_{lz}\}^T \quad \{M_l\} = \{M_{lx}\ M_{ly}\ M_{lz}\}^T \quad l = 1, 2 \quad (19)$$

The influence from inertia forces on the damper may normally be neglected, which gives:

$$\{F_0\} = \{0\ 0\ F_c\}^T \qquad \{M_0\} = \{0\ 0\ 0\}^T \qquad (20)$$

where F_c is the centrifugal load induced by damper mass and disk rotational speed. Balance of forces and moments on the damper is formulated as:

$$\{F_0\} + \{F_1\} + \{F_2\} = \{0\} \qquad (21)$$

$$\{M_0\} + \{M_1\} + \{M_2\} + \{r_1\} \times \{F_1\} + \{r_2\} \times \{F_2\} = \{0\} \quad (22)$$

where $\{r_1\} = \{-a_1\ 0\ b_1\}^T$ and $\{r_2\} = \{a_2\ 0\ b_2\}^T$ are position vectors from centre of gravity to contacts C_1 and C_2. Displacement and rotation of damper contacts C_1 and C_2 are defined in two parts, a rigid body motion with superscript r and an elastic deformation with superscript e.

$$\{\varphi_l\} = \{\varphi_0\} + \{\varphi_l^e\} \qquad \{u_l\} = \{u_l^r\} + \{u_l^e\} \qquad l = 1, 2 \quad (23)$$

where the rigid body displacement is found as

$$\{u_l^r\} = \{u_0\} + \{\varphi_0\} \times \{r_l\} \qquad (24)$$

The stiffness of the damper "body" may for instance be found from a finite element model of the damper. Stiffness matrices for C_1 and C_2 are defined using C.G. as a fixed point. Forces due to elastic deformation are then found as

$$\begin{Bmatrix} F_l \\ M_l \end{Bmatrix} = [K_l] \begin{Bmatrix} u_l^e \\ \varphi_l^e \end{Bmatrix} \qquad (25)$$

Solution Algorithm

Equations from previous sections are formed into a solution algorithm. Input data are displacement and rotation of blade platforms as functions of time and output data are damper displacements and contact forces. The set of equations cannot be solved directly because the contact forces are nonlinear. Instead we implement the algorithm into a computer program and use a nonlinear least-square method found in a commercial software package to solve it. The algorithm contains the following steps:

1 Assume rigid body motions $\{u_0\}$ and $\{\varphi_0\}$

2 Assume elastic deformation $\{u_l^e\}$ and $\{\varphi_l^e\}$

3 Compute damper displacement $\{u_l\} = \{u_0\} + \{u_l^e\}$

4 The rotation of the bristles is divided into two parts: a rigid body rotation around *C.G.* and a rotation around global system 1 or 2 due to damper elasticity and platform rotation. Rotated and translated bristle attachment points are found as shown in the first box of the algorithm in Figure 10.

5 Compute normal and traction forces as shown in Figure 10.

Steps 2 to 5 are done for both contact interfaces that is $l = 1$ and 2.

6 Transform forces and moments to global coordinate system

7 Equilibrium of forces on damper

8 Equilibrium of contact forces and damper deformations

We have in the general case 3 global nodes on the damper and 6 DOF, where the nodes are: *C.G.*, C_1 and C_2. This gives 18 unknowns and consequently the same number of equations to solve iteratively at every time step.

The damper used for simulations and experiments in this paper was developed at Volvo Aero Corporation in Trollhättan, Sweden. A cross section of the damper is shown in Figure 4. This damper has one contact radius and the nominal contact area will be a line contact. One should note that there will not be line contact if the damper is rotated $\varphi_{0,x}$ or $\varphi_{0,y}$. Input data for the Brush model are found from the damper geometry, material parameters and measured coefficients for friction and tangential stiffness. Variables remaining to be identified are the stiffnesses of the damper "body". These were found using a finite element model of the damper. Three stiffnesses were identified as important to incorporate in the damper model: $k_{xx1} = k_{xx2}$, $k_{yy1} = k_{yy2}$ and $k_{mzz1} = k_{mzz2}$, where index m indicates that this is a torsion stiffness. The damper is considered to be rigid in all other degrees of freedom. This gives 12 equations to solve at every time step.

One "problem" with this damper model occurs when both contact area C_1 and C_2 perform macroslip in the same direction. The displacement of the damper will be undetermined if forces do not change for a change of platform displacement. This problem is overcome by setting the coefficient of friction slightly higher on one of the contact areas.

FORCED RESPONSE ANALYSIS

A forced response simulation may be conducted in the time domain, in the frequency domain or by using an alternating method, Cameron and Griffin [26]. Time-marching or time-domain simulations require a lot more cpu time than frequency-domain simulations and it is therefore better to use the latter method if possible. The agreement of time- and frequency-domain simulations has been investigated by many researchers, see for instance [7], [8], [16], Menq and Griffin [27] and Sanliturk *et al.* [28]. They all showed good agreement of the two methods, although [8] showed that the frequency-domain solution gives an optimal damper weight that is slightly lighter than given by the time-domain result. The weight of the damper gives the centrifugal force F_c and the optimal weight is the one that minimizes the forced response. We will thus do simulations in the frequency domain.

Equivalent stiffness and damping

In order to use the frequency domain we need to linearize the friction damper. The harmonic balance method, HBM, is the most commonly used linearization method in friction damping analysis. We shall only review the basic concept of the method here. A more thorough discussion can be found in [7]. There will be a nonlinear response to a harmonic excitation for a nonlinear system. The response may be expanded as a Fourier series. In HBM one assumes that the first sine and cosine terms of the Fourier expansion dominate, and all higher order terms are neglected. One may say that HBM transforms nonlinear differential equations into nonlinear algebraic equations, which are solved faster. The damper may then be expressed as a complex stiffness $k^*_{damp} = k_{eq} + ic_{eq}$. The real part of the complex damper stiffness may be seen as an equivalent stiffness coefficient and the imaginary part may be seen as an equivalent damping coefficient. The HBM is here utilized by tracing platform forces and damper displacements for typically two periods of motion when the platforms are subjected to a relative motion.

We see in Figure 19 linearized properties k_{eq} and c_{eq} plotted as functions of relative platform displacement amplitude u_{amp} for two damper models.

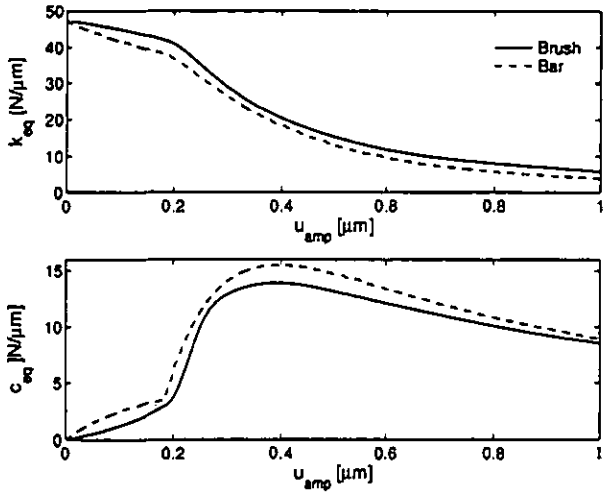

Figure 19 Comparison of equivalent stiffness and damping for Bar and Brush models. Normal force on damper N = 100N. Radius r_x = 2.6 mm for Brush model.

Curves labelled "Bar" are for a damper model presented in paper [8], and shown in Figure 20. The model consists of two Bar model friction interfaces, and a spring between them. The spring has nominally the same stiffness as the one shown in Figure 18.

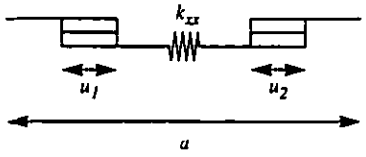

Figure 20 The Bar friction damper model.

If we consider the normal force and coefficient of friction as given, then the variables for the Bar damper model are: A, l and k_{xx}. These were varied from the original estimation to give as good fit as possible to the stiffness and damping curves of the Brush model. It is seen in Figure 19 that the Bar model gives less stiffness and more damping than the Brush model. The two models approach the same damping as the relative displacement, u_{amp}, increases e.g. when there is more macroslip and less microslip, this is as expected. The difference in stiffness between the models is, however, approximately constant. The overall agreement between the two damper models is, however, acceptable, which indicates that the Bar model may be used for one-dimensional slip motion.

How changing the normal force, N, and damper stiffness, k_{xx}, affects the linearized properties is shown in Figure 21. Simulations were made for the following normal loads: N = 10, 20, 50 and 100 N. There may in some cases be a coupling between normal load and damper stiffness. This is discussed in section . The damper stiffnesses used were: k_{xx} = 17, 33, 67 and 100 N/mm. The appearance of the curves is very similar. They may in fact be scaled to align on one curve if we introduce nondimensional variables: displacement $u_{amp}k_{xx}/N$, stiffness k_{eq}/k_{xx} and damping c_{eq}/k_{xx}.

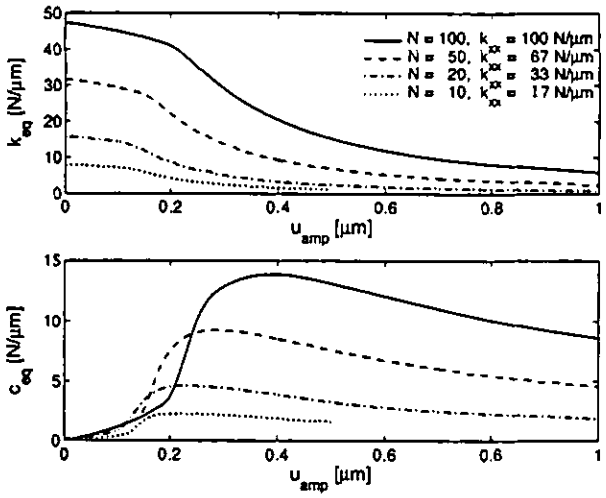

Figure 21 Equivalent stiffness and damping for Brush damper model. Variation of normal force N and damper stiffness k_{xx}

One should, however, note that this is a simulation case with only one-dimensional slip, no rolling and constant normal load. These nondimensional variables may not be used in the general case. These simulation results are used in the next section where experiments are compared with simulations.

Verification of damper model

In order to verify the Brush damper model and investigate the influence of changing damper contact radius, the experiment set-up in Figure 22 was used. Access to the blade-damper-blade test rig was provided by *Centre of Vibration Engineering* at *Imperial College*. Tests were made using ICATS MODACQ, which is a computer software used for controlled-input, stepped-sine testing. Sanliturk *et al.* developed this test rig to verify a 2D friction interface model in [29] and revised it to verify the cottage roof damper model in [17], which is exactly the same rig as used in this paper. The only difference is of course the damper.

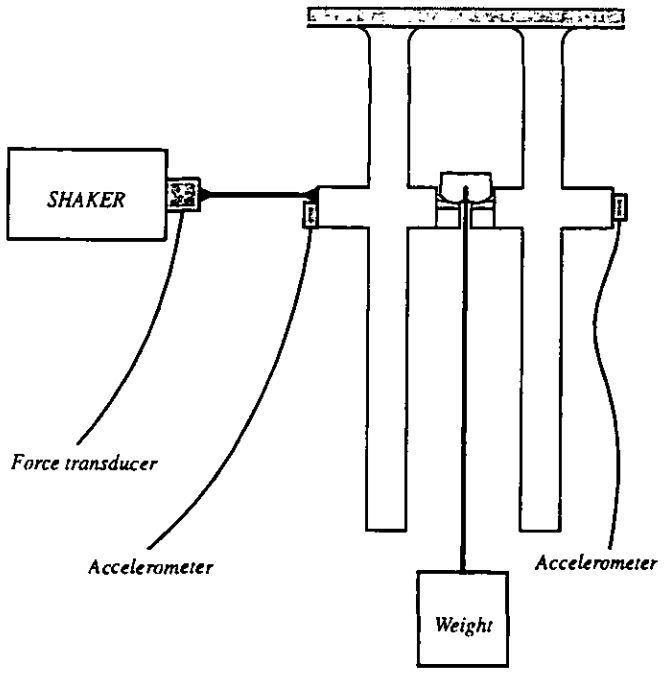

Figure 22 Experimental set-up: Two beams with a damper in between. The left beam is exited by a shaker and response is measured for both beams.

The test beams, simulating two turbine blades, are tuned to have the same natural frequency and are bolted together on a big inertia block. The damper is positioned in between the two blades and a piece of a real turbine blade platform (shown as a grey wedge in Figure 22) is glued on each beam platform. This gives the right material combination between damper and blade and the opportunity to change the platform angle. The damper normal force, which is the counterpart of the centrifugal force in the actual engine operation, was applied by an elastic string and a number of weights. One of the beams was excited with a shaker. The excitation force was measured with a force transducer and controlled to be equal to F_{ex} = 1N by a computer. The displacements of the two beams was measured with accelerometers. The first bending mode for the beams was studied for damper normal loads N = 10, 20, 50 and 100N and for damper radius r_x = 2.6, 5 and 10 mm. Measured responses are shown in the figures in the next section. Only data for the beam excited by the shaker are displayed here. The other beam showed similar response, except that there was no anti-resonance.

A beam element model was used for simulations in the frequency domain. The governing equation for the dynamic system is

$$[P^*] = [E^*(\omega)]\{p^*\} \qquad (26)$$

Vectors $\{P^*\}$ and $\{p^*\}$ are complex force and displacement amplitudes respectively. The matrix $[E^*(\omega)]$ is the dynamic stiffness matrix and is a function of excitation frequency ω. The stiffness of one beam element is defined using the so called Kolousek's functions [30] for a damped Timoshenko beam, Lundén and Åkesson [31]. Beam stiffness matrices together with the complex stiffness of the damper k^*_{damp} are assembled into the dynamic stiffness matrix of the beam and damper system. Damper stiffness is a function of the relative displacement between the two beam platforms and the variable for which Eq. (26) is solved iteratively. The results from simulations are for comparison shown in the same figures and tables as the experimental results.

Experiment and simulation results

The most common way to display forced response results is by making tracking plots, where the amplitude displacement is plotted as a function of excitation frequency. A family of tracking plots with experimental and simulation results are shown in Figures 23 and 24. The corresponding response data at resonance are shown in Tables 1 and 2.

The first bending modes of the beams were studied. There are two resonance peaks in the frequency range of interest. They occur at 536 and 544 Hz if the system is excited without the damper being present. There will still be a small coupling of the beams via the inertia block. The lower frequency is an in-phase mode and the higher frequency is an out-of-phase mode. The major effect of the friction damper is on the out-of-phase mode, as seen in the figures. The damping effect on the in-phase mode is insignificant. The simple reason is that there is virtually no relative motion between beam platforms for the in-phase mode and thus no motion of the damper.

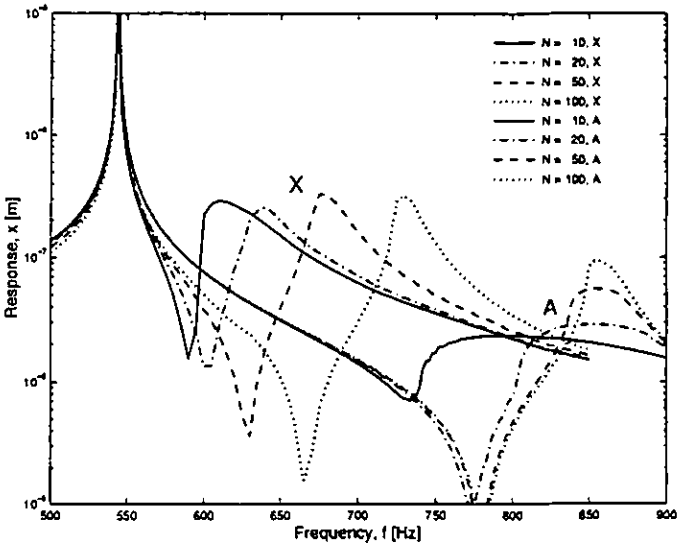

Figure 23 Tracking plots for damper with r_x = 2.6 mm, experiment (X) vs. analysis (A)

Table 1 Response at resonance for damper radius r_x = 2.6 mm

	Experiment		Analysis	
N	f [Hz]	x [μm]	f [Hz]	x [μm]
10	610	0.29	800	0.02
20	640	0.26	850	0.03
50	675	0.33	855	0.06
100	730	0.32	855	0.09

Figure 23 shows tracking plots for the damper with radius r_x = 2.6 mm. Response data at resonance are displayed in Table 1. We see that the agreement between simulated and measured response is not so good.

One may observe three facts:

- Resonance occurs at higher frequencies and with lower amplitude for simulations than for experiments.
- The shift in resonance frequency when the damper normal force increased from N = 10N to N = 100N is less for analysis than for experiments.
- Normally one expects to find an optimal normal force which minimizes the response at resonance. Simulations show that the optimal force is probably close to 10N, while the amplitude at resonance is approximately constant in the experiments.

These facts suggest that there are effects in the experiments which are not included in simulations. It may also be noted that displacements are very small, less than one micro-meter and that it is difficult to get accurate measurements for such a small displacement.

An inspection of damper contact surfaces showed that there had been contact along approximately 6 mm out of 13 mm, which is the length of the damper. This effect not only the parameters for the Brush model, but also the stiffness of the damper "body", k_{xx}. To determine what the contact length was for different normal forces is difficult, but we make a first guess to see how it affects the simulations. It is assumed that the contact length is a function of normal force so that N = 10, 20, 50 and 100N give l_y = 1, 2, 4 and 6 mm respectively. Another assumption is that the damper stiffness is a function of contact length, giving k_{xx} = 17, 33, 66 and 100 N/μm. The resulting damper stiffness and damping functions are shown in Figure 21. Response curves are depicted in Figure 24 and resonance data are shown in Table 2.

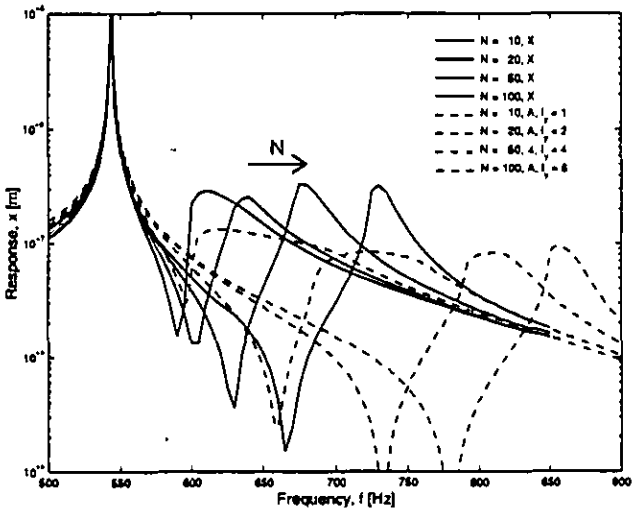

Figure 24 Tracking plots for damper with r_x = 2.6 mm. Experiment (X) vs. analysis (A) varying damper stiffness and contact length.

Simulation results show better agreement now. The shift in resonance frequency is larger than from previous analysis and the resonance amplitude is approximately constant for the four set-ups of damper variables. The parameter that has the largest influence on simulation results for these cases is the effective damper stiffness. This is due to the fact that relative displacement in the friction joint is small and the other variables have less effect when there is little slip. Changing damper stiffness has little influence on resonance amplitude for these cases. It is seen in Table 2 that the amplitude is about three times higher in the experiments and the shape of the response curves indicates that the damping is less in the experiments than in simulations. This has yet to be explained.

Table 2 Response at resonance when damper stiffness and contact length vary.

	Experiment		Analysis	
N	f [Hz]	x [μm]	f [Hz]	x [μm]
10	610	0.29	610	0.13
20	640	0.26	700	0.08
50	675	0.33	805	0.08
100	730	0.32	855	0.09

Discussion of experimental and simulation results

The comparison of simulation and experimental results shows that the contact length between damper and platform varies with the normal load. This effect is not included in the Brush model, where it is assumed that all bristles have equal unloaded length e.g. the surfaces in contact are smooth. Changing the normal force will not affect the contact length if there is line contact. Surface roughness is modelled if one considers the bristles as asperities and give them a distribution of unloaded length. It is also necessary to include wear in the contact model if surface roughness is considered. Modelling of elastic contact with wear is an important field of research, see for instance Strömberg [32] and Hagman [33], which also includes measurements of microslip. Including surface finish and wear will make the damper model rather complex, especially for use in dynamic simulations. The best way of solving this problem is probably to have two models: one more complex for wear simulations and one which is less complete, but may be used in dynamic simulations. The two models should than be calibrated against each other.

Not having contact on the whole damper surface will probably not need to be considered when simulations are made on the real jet engine case. This is due to the fact that both normal and excitation forces on the damper are about ten times higher than what was used in the experiments and simulations in this paper. Applying such a high normal load is very difficult when using a test rig that is not spinning.

Another objective of the experiments, besides verifying the damper model, was to investigate the influence of damper radius r_x on the forced response. Experiments showed that making the damper contact surface flatter i.e. making r_x larger, will give a small increase in resonance frequency and a small decrease in resonance amplitude. This would imply that the best damping effect is found by making the contact radius larger and ultimately making the contact surface flat which is a cottage roof damper. There is, however, another effect of increasing the damper radius that does not appear in measurements. There was a problem aligning in the damper with r_x = 10 mm. The damper had a tendency during the vibration test to roll over so that the contact on one side would not be on the curved surface, but on the edge where the curved surface ended, causing the damper to jam. The r_x = 5 mm damper also had the tendency to roll over but the effect was less obvious. The alignment problem has also been observed in simulations. It occurs if the phase angle between the motion of left and right platforms is small. The

damper displacement will then drift away although the applied platform displacement is cyclic. The rolling effect has also been observed and addressed for the cottage roof damper in [17].

CONCLUSIONS

A friction interface model where the mating surfaces are curved has been developed in this paper. The interface model is based on a discretization of the Winkler elastic foundation contact model and is named the Brush model. This model is general in the sense that it allows for effects such as two-dimensional slip, variable normal load and rolling. All variables for the contact model are based on damper geometry and material data, except coefficient of friction and tangential stiffness coefficient, which have to be measured. Simulated and experimental hysteresis curves for the Brush model are reported.

A model of a curved wedge damper has been developed using the Brush model. The damper can move in all six degrees of freedom. This damper has nominally line contact between damper and blade platform. An algorithm for solving damper forces and displacements has been presented. The governing equations are solved using a nonlinear least-square method routine in a commercial software package.

The damper is linearized using the harmonic balance method and represented as a complex stiffness which is a function of relative displacement between blade platforms. This makes the damper easy to use in forced response analysis in the frequency domain.

Experiments were made with a beam-damper-beam set-up. Comparison with simulations showed there was not contact along the whole damper length. This resulted in problems in getting agreement between experiments and simulations. Experiments are probably influenced by surface roughness, which is not included in the Brush model. Not having contact on the whole damper surface is probably not a problem when simulations are made on the real jet engine case. This is due to the fact that both normal and excitation forces on the damper are about ten times higher than what was used in the experiments and simulations in this paper.

Variation of contact radius of the damper shows that a larger radius i.e. a flatter contact gives better damping and increases the resonance frequency. The disadvantage is that the alignment of the damper becomes more unreliable. Recommendations for future work with the Brush model are:

- Implement variation of unloaded bristle length. This is needed for studying the effect of contact surface roughness.
- Develop theory for finding the tangential stiffness coefficient without using experiments.
- Determine how partial contact affects the stiffness between the two contact areas for the curved damper model.

ACKNOWLEDGMENTS

The theoretical work has been carried out at Linköping University, Department of Mechanical Engineering, Division of Machine Design in Linköping, Sweden. The author wishes to thank Professor Karl-Olof Olsson, Head of the Division of Machine Design, for his helpful discussions and support.

The experimental work has been carried out at Imperial College of Science, Technology and Medicine, Centre of Vibration Engineering, London, UK and the author is most grateful for being given access to the experimental facilities and would like to acknowledge A.B. Stanbridge for all the support he has given during that part of the work.

This work was financially supported by the National Aeronautical Research Program under grant NFFP-244 and has also been associated with a research programme "Mechanical Friction Damping" performed at Imperial College, supported by Rolls-Royce Aerospace Group. The author wants to thank Professor D.J. Ewins and Dr. K.Y. Sanliturk at Imperial College for sharing their experience and knowledge in fruitful discussions.

The author would like to thank the people at the Volvo Aero Corp., Military Engines and especially Mr. Magnus Andersson for their interest and encouragement.

REFERENCES

[1] Griffin J.H., 1990, "A Review of Friction Damping of Turbine Blade Vibration," *International J. of Turbo and Jet Engines*, Vol. 7, pp. 297-307

[2] den Hartog J.P., 1931, "Forced Vibrations with Combined Coulomb and Viscous Damping." *Trans. ASME* 53, APM:107-115

[3] Griffin J.H., "Friction Damping of Resonant Stresses in Gas Turbine Engine Airfoils", *ASME J. of Engineering for Power*, Vol. 102, Apr., pp. 329-333

[4] Mindlin R.D., Mason W.P., Osmer J.F., Deresiewicz H, 1952, "Effects of an Oscillating Tangential Force on the Contact Surfaces of Elastic Spheres", 1st US National Congress of Applied Mechanics (Chicago III, 1951), New York, ASME, pp. 203 - 208

[5] Metherell A.F., Diller S.V., 1968, "Instantaneous Energy Dissipation Rate in a Lap Joint - Uniform Clamping Pressure", *Trans. ASME, J. of Applied Mechanics*, pp. 123 - 128

[6] Menq C.H., Beilak J., Griffin J.H., 1986, "The Influence of Microslip on Vibratory Response, Part I: A new Microslip Model." *J. of Sound and Vibration*, Vol. 107(2), pp. 279 - 293

[7] Csaba G., 1995, "Microslip Friction Damping with Special Reference to Turbine Blade Vibrations", LiU-Tek-Lic-1995:09, ISBN 91-7871-507-5, Linköping University, Sweden

[8] Csaba G., 1998, "Forced Response Analysis in Time and Frequency Domain of a Tuned Bladed Disk with Friction Dampers", *J. of Sound and Vibration*, Vol. 214(3), pp. 395-412

[9] Csaba G., Andersson M., 1997, "Optimization of Friction Damper Weight, Simulation and Experiments", *ASME Turbo Expo 1997*, Orlando, Florida USA, June 2-5 1997, paper 97-GT-115

[10] Srinivasan A.V., Cutts D.G., 1984, "Measurement of Relative Vibratory Motion at the Shroud Interfaces of a Fan", *J. of Vibration, Acoustics, Stress and Reliability in Design*, Vol. 106, pp. 189 - 197

[11] Menq C.H., Chidamparam P., Griffin J.H., 1991, "Friction Damping of Two-Dimensional Motion and its Application in Vibration Control", *J. of Sound and Vibration*, Vol. 144(3) pp. 427 - 447

[12] Sanliturk K.Y., Ewins D.J., 1996, "Modelling Two-Dimensional Friction Contact and its Application using Harmonic Balance Method", *J. of Sound and Vibration*, Vol. 193(2), pp. 511- 523

[13] Sextro W., Popp K., Wolter I., 1997, "Improved Reliability of Bladed Disks due to Friction Dampers.", *ASME Turbo Expo 1997*, Orlando, Florida USA, June 2-5 1997, paper 97-GT-189

[14] Pfeiffer F., Hajek M., 1992, "Stick-slip Motion of Turbine Blade Dampers", Phil. Trans. R. Soc. London A 338, pp. 503 - 517

[15] Yang B.D., Menq C.H., 1997, "Characterization of Contact Kinematics and Application to the Design of Wedge Dampers in Turbomachinery Blading, Part I: Stick-slip Contact Kinematics", *ASME Turbo Expo 1997*, Orlando, Florida USA, June 2-5 1997, paper 97-GT-19

[16] Yang B.D., Menq C.H., 1997, "Characterization of Contact Kinematics and Application to The Design of Wedge Dampers in Turbomachinery Blading, Part II: Prediction of Forced Response and Experimental Verification", *ASME Turbo Expo 1997*, Orlando, Florida USA, June 2-5 1997, paper 97-GT-19

[17] Sanliturk K.Y., Ewins D.J., Stanbridge A.B., 1999, "Underplatform dampers for turbine blades: Theoretical modelling, analysis and comparison with experimental data", *ASME Turbo Expo 1999*, Indianapolis, Indiana, USA, June 7-10, paper 99-GT-

[18] Srinivasan A.V., Cassenti B.N., 1986, "A Nonlinear Theory of Dynamic Systems With Dry Friction Forces", *J. of Engineering for Gas Turbines and Power*, Vol. 108, pp 525 - 530

[19] Pödra P., Andersson S., 1997, "Wear Simulation with the Winkler Surface Model", *WEAR*, Vol. 207, pp.79 - 85.

[20] Johnson K.L., 1985, "Contact Mechanics", Cambridge University Press

[21] Pärletun L.G, Hansson P., Karlsson G., 1989, "Datorgrafik och CAD-teknik", Studentliteratur, Lund Sweden, ISBN 91-44-28591-4, In Swedish

[22] Iwan W.D., 1967, "On a Class of Models for the Yielding Behaviour of Continuous and Composite Systems", *J. of Applied Mechanics*, Sept. 1967, pp. 612-617

[23] Menq C.H., Griffin J.H., Bielak J., 1986, "The Forced Response of Shrouded Fan Stages", *J. Vibration, Acoustics, Stress and Reliability in Design*, Vol. 108, pp. 50 - 55

[24] Yang B.D., Menq C.H., 1996, "Modeling of Friction Contact and its Application to The Design of Shroud Contact", *ASME Turbo Expo 1996*, Birmingham, UK, June 10-13 1996, paper 96-GT-472

[25] Sanliturk K.Y., Stanbridge A.B., Ewins D.J., 1995, "Friction dampers: Measurement, Modelling and Application to Blade Vibration Control", 1995 ASME Design Engineering Technical Conference, Vol. 3, Part B, pp.1377-1382

[26] Cameron T.M., Griffin J.H., 1989, "An Alternating Frequency/ Time Domain Method for Calculating the Steady-State Response of Nonlinear Dynamic Systems", *J. of Applied Mechanics*, Vol. 56, pp. 149 - 154

[27] Menq C-H., Griffin J. H., 1985, "A Comparison of Transient and Steady State Finite Element Analyses of The Forced Response of a Frictionally Damped Beam," *J. of Vibration, Acoustics, Stress and Reliability in Design*, Vol. 107, pp. 19 - 25

[28] Sanliturk K.Y., Imregun M., Ewins D.J., 1997, "Harmonic Balance Vibration Analysis of Turbine Blades with Friction Dampers", *Trans. ASME, J. of Vibratian and Acoustics*, Vol. 119, pp. 96 - 103

[29] Sanliturk K.Y., Stanbridge A.B., Ewins D.J., 1996, "Friction Damper Optimization for Turbine Blades: Experiment and Theoretical Predictions", IMechE, C500/019/96, pp. 171 - 186

[30] Kolousek V., 1973, "Dynamics in Engineering Structures", Butterworths, London

[31] Lundén R., Åkesson B., 1983, "Damped Second-order Rayleigh-Timoshenko Beam Vibration in Space - An Exact Complex Dynamic Member Stiffness Matrix", *J. for Numerical Methods in Engineering*, Vol. 19, pp. 431 - 449

[32] Strömberg N., 1997, "Thermomechanical Modelling of Tribological Systems", Doctoral Thesis at the Div. of Mechanics, Dept. of Mechanical Engineering, Linköping University, Sweden, ISBN 91-7219-013-2, ISSN 0345-7524

[33] Hagman L.A., 1997, "Measurement and Modelling of Microslip for Engineering Surfaces in Contact", Doctoral Thesis at the Dept. of Machine Elements, The Roy. Inst. of Technology, Stockholm, Sweden, TRITA-MMK 1997:11, ISSN 1400-1179